

# Field-induced Kitaev multipolar liquid in spin-orbit coupled $d^2$ honeycomb Mott insulators

 Ahmed Rayyan<sup>1</sup>, Derek Churchill<sup>1</sup> and Hae-Young Kee<sup>1,2,\*</sup>
<sup>1</sup>*Department of Physics, University of Toronto, Toronto, Ontario, Canada M5S 1A7*
<sup>2</sup>*CIFAR Program in Quantum Materials, Canadian Institute for Advanced Research, Toronto, Ontario, Canada M5G 1M1*


(Received 27 June 2022; accepted 16 December 2022; published 23 January 2023)

The Kitaev model, characterized by bond-dependent Ising spin interactions among spin-orbit entangled dipole moments in Mott insulators, offered a new approach to quantum spin liquids. Motivated by another type of bond-dependent interaction among quadrupole moments in  $5d^2$  Mott insulators, we provide a microscopic route to uncover the Kitaev multipolar liquid, featuring fractionalized excitations out of non-Kramers doublets carrying multipole moments. The key ingredient is the magnetic field that allows for bond-anisotropic quadrupole-octupole interactions via mixing with the excited triplet states. The conditions to realize signatures of this phase in real materials are also discussed.

 DOI: [10.1103/PhysRevB.107.L020408](https://doi.org/10.1103/PhysRevB.107.L020408)

**Introduction.** Recently, there have been many studies on candidate materials of Kitaev spin liquids (KSLs) as they offer a platform for topological quantum computation [1,2]. The Kitaev honeycomb model consists of bond-dependent Ising interactions leading to the KSL with Majorana fermion and  $\mathbb{Z}_2$  vortex excitations. It was shown that bond-dependent (or “compass”) interactions appear naturally in Mott insulators with strong spin-orbit coupling since the spin sector of the localized wave functions becomes sensitive to the orbital spatial orientation due to spin-orbit entanglement [3–12]. Since then there has been an intensive search for candidate Kitaev materials described by an effective model of spin-orbit entangled  $J_{\text{eff}} = 1/2$  Kramers doublets [3,4,9,13–31].

Bond-dependent interactions are not limited to Kramers doublets; in the  $5d^2$  double perovskites, the  $J = 2$  states are further split into a non-Kramers doublet and an excited triplet via  $t_{2g}$ - $e_g$  mixing [32–34]. The non-Kramers doublet hosts quadrupole and octupole moments while lacking a dipole moment, and the microscopic theory of the multipolar interactions exhibit octupole-octupole and bond-dependent quadrupole-quadrupole interactions [35–37]. Remarkably, such interactions on the honeycomb lattice take the form of the extended Kitaev model, which includes the bond-dependent off-diagonal exchanges  $\Gamma$  and  $\Gamma'$  along with the conventional Heisenberg interaction. Given their similarity, one may question if there is a way to realize the exactly solvable Kitaev model in multipolar honeycomb systems.

In this Letter, we present a microscopic theory to uncover the Kitaev model among multipolar moments where non-Kramers doublets are fractionalized into Majorana fermions and  $\mathbb{Z}_2$  vortices; we call this phase the *Kitaev multipolar liquid* in analogy with the KSL. The key ingredient to realize the KML is the application of a magnetic field which leads to bond-dependent quadrupole-octupole interactions ordinarily forbidden by time-reversal symmetry. Below we first derive

the low-energy effective multipolar model including the time-reversal symmetry breaking terms and present its classical phase diagram. Noticing a special point in the phase diagram which maps to the pure antiferro-Kitaev model, we investigate the extent of the KML in the quantum phase diagram using exact diagonalization (ED) on the 24-site cluster. We summarize our results and discuss the conditions to realize signatures of the KML in  $d^2$  honeycomb insulators.

**Multipolar pseudospin-1/2 interactions.** Electronic states of transition metal ions enclosed in an octahedral cage are generally split by cubic crystal fields into a low-lying  $t_{2g}$  triplet and an excited  $e_g$  doublet. For a  $d^2$  filling, the orbital sector is described by three antisymmetrized two-electron states, forming an effective total angular momentum  $L = 1$  which is then coupled to the total spin  $S = 1$  via spin-orbit coupling, resulting in the  $J = 2$  multiplet [38]. The  $J = 2$  dipole operators are given by  $J_\gamma = \hat{\mathbf{e}}_\gamma \cdot \mathbf{J}$  for  $\gamma \in \{x, y, z\}$ , where  $\hat{\mathbf{e}}_{x,y,z}$  point along the three anion directions; see Fig. 1(a). The fivefold-degenerate  $J = 2$  state can then be further split by virtual processes mixing the electronic  $t_{2g}$  and  $e_g$  states via spin-orbital excitations, resulting in a ground state doublet and excited triplet separated by energy gap  $\Delta$ ; see Fig. 1(b). In analogy with the five electronic  $d$  orbital states, we refer to the doublet and triplet states as  $E_g$  and  $T_{2g}$ , respectively. The  $E_g$  doublet is of the non-Kramers type with vanishing magnetic dipole moment, but carries higher-rank moments, i.e., quadrupole and octupole moments denoted by the operators  $Q_{x^2-y^2} = J_x^2 - J_y^2$ ,  $Q_{3z^2} = (3J_z^2 - \mathbf{J}^2)/\sqrt{3}$ , and  $T_{xyz} = \frac{\sqrt{15}}{6} \overline{J_x J_y J_z}$ , where the overline symbol denotes symmetrization of the underlying operators. Let us define three operators  $s^{a,b,c}$  as

$$(s^a, s^b, s^c) \equiv \frac{1}{2} \mathcal{P}_{E_g}^\dagger \left( \frac{Q_{3z^2}}{2\sqrt{3}}, \frac{Q_{x^2-y^2}}{2\sqrt{3}}, \frac{T_{xyz}}{3\sqrt{5}} \right) \mathcal{P}_{E_g}, \quad (1)$$

where  $\mathcal{P}_{E_g}$  is the projection operator onto the  $E_g$  doublet. The action of these operators on the  $E_g$  subspace can be represented by the three Pauli matrices  $(s^a, s^b, s^c) =$

\*hykee@physics.utoronto.ca

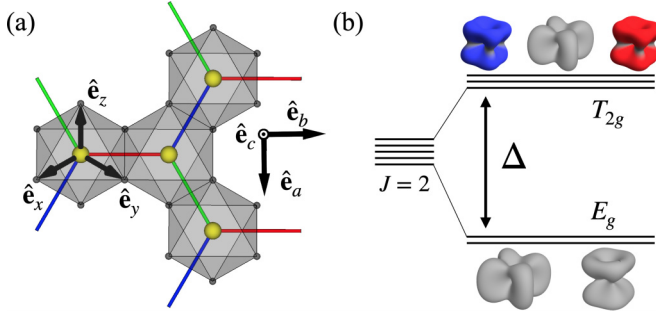


FIG. 1. (a) Honeycomb lattice with transition metal ions (shown in yellow) enclosed in an octahedral anion cage (shown in gray). The crystallographic  $abc$  and octahedral  $xyz$  coordinates are shown. The  $x$ ,  $y$ ,  $z$  bonds are colored green, blue, and red, respectively. (b) Single-ion level scheme for the  $J = 2$  moment. The fivefold degeneracy is split by an energy gap  $\Delta$  into a low-lying non-Kramers  $E_g$  doublet and an excited  $T_{2g}$  triplet by electronic  $t_{2g}$ - $e_g$  mixing induced by spin-orbit coupling [32,34]. The  $E_g$  and  $T_{2g}$  states are also shown where red and blue represent nonzero spin density.

( $\sigma^3$ ,  $\sigma^1$ ,  $\sigma^2$ )/2, so that  $s^{a,b,c}$  form effective pseudospin-1/2 operators. The components are given by  $s^{\tilde{\gamma}} = \hat{\mathbf{e}}_{\tilde{\gamma}} \cdot \mathbf{s}$  for  $\tilde{\gamma} \in \{a, b, c\}$ , where  $\hat{\mathbf{e}}_c$  points out of the honeycomb plane spanned by  $\hat{\mathbf{e}}_a$  and  $\hat{\mathbf{e}}_b$ ; see Fig. 1(a). The quadrupolar and octupolar moments are in one-to-one correspondence with the projection of  $\mathbf{s}$  onto the  $ab$  plane or the  $c$  axis, respectively.

We now investigate the form of the multipolar interactions by introducing  $t_{2g}$  orbital hopping, as was done in the case of the  $d^2$  double perovskites [35–37]. On a honeycomb  $z$  bond, the parameters  $t_3$  and  $t_1$  represent intraorbital hopping through  $xy - xy$  overlap, or  $xz - xz$  and  $yz - yz$  overlaps, respectively; see Fig. 1 of the Supplemental Material (SM) [39]. We also introduce an  $xz - yz$  interorbital hopping through the edge-shared anions by hopping parameter  $t_2$ . We go beyond earlier studies by immersing the system in an external magnetic field  $\mathbf{h} = (h^x, h^y, h^z)$ . The spin and orbital degrees of freedom are sensitive to this field via a Zeeman coupling  $H^Z = \mu_B(\mathbf{L} + 2\mathbf{S}) \cdot \mathbf{h} = g_J \mu_B \mathbf{J} \cdot \mathbf{h}$ , which introduces off-diagonal matrix elements between the doublet and triplet states [39]. We ensure that the  $E_g$  and  $T_{2g}$  manifolds remain well separated by considering the low-field limit  $g_J \mu_B |\mathbf{h}| \ll \Delta$  so that the perturbative expansion is carried out in both  $|\mathbf{h}|/\Delta$  and  $t_{ij}^2/U$ , where  $t_{ij}$  is some hopping between sites  $i$  and  $j$  and  $U$  is the Hubbard energy cost of double occupancy. The external field gives rise to new virtual processes where the  $E_g$  doublet mixes with the polarized  $T_{2g}$  triplet during the hopping procedure; see Fig. 2. This process generates new terms in the effective Hamiltonian denoted by  $J_B^{\gamma}$  and  $\mathbf{h}_{\text{eff}} = (h_{\text{eff}}^a, h_{\text{eff}}^b, h_{\text{eff}}^c)$  appearing at third order in addition to the previously derived  $J_{\tau}$ ,  $J_Q$ , and  $J_O$ :

$$H = \sum_{\langle ij \rangle_{\gamma}} J_{\tau} \tau_i^{\gamma} \tau_j^{\gamma} + J_Q (s_i^a s_j^a + s_i^b s_j^b) + J_O s_i^c s_j^c - \sqrt{2} J_B^{\gamma} (\tau_i^{\gamma} s_j^c + s_i^c \tau_j^{\gamma}) - \sum_i \mathbf{h}_{\text{eff}} \cdot \mathbf{s}_i, \quad (2)$$

where  $\tau^{\gamma} \equiv s^a \cos \phi_{\gamma} + s^b \sin \phi_{\gamma}$  is a compass quadrupole operator with  $\phi_{\gamma} = 0, 2\pi/3, 4\pi/3$  for a given bond of type  $\gamma = z, x, y$ . Crucially, the addition of a magnetic field

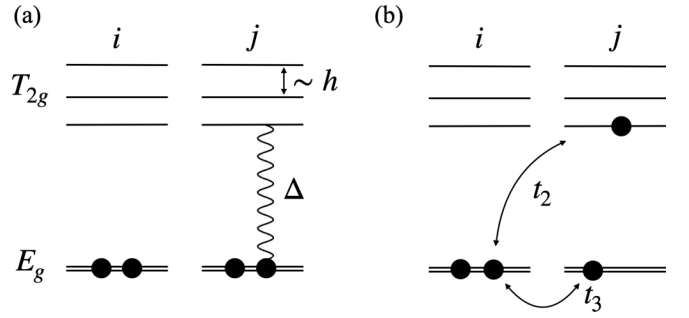


FIG. 2. Schematic of a virtual process that contributes to both  $J_B$  and  $h_{\text{eff}}$  term in the effective Hamiltonian Eq. (2) at third order for the case of a magnetic field aligned along the  $c$  axis. The  $E_g$  and  $T_{2g}$  states at site  $j$  mix due to (a) the on-site Zeeman field and (b) hopping of an electron via interorbital  $t_2$  and intraorbital  $t_3$ ; see visual representation of the orbital overlaps in Fig. 1 of the SM [39]. The overall contribution is then proportional to  $(t_2 t_3 / U)(h / \Delta)$ .

supplements the Hamiltonian of Ref. [37] with terms ordinarily forbidden by time-reversal symmetry, including a bond-anisotropic quadrupole-octupole interaction  $J_B^{\gamma}$ ; that is,  $J_B^x$ ,  $J_B^y$ , and  $J_B^z$  generally differ in strength along each bond. For the case of a [111] magnetic field  $\mathbf{h} = h \hat{\mathbf{e}}_c$ , the  $J_B^{\gamma}$  interaction becomes bond isotropic with  $J_B \equiv J_B^x = J_B^y = J_B^z$ , and  $h_{\text{eff}}^a = h_{\text{eff}}^b = 0$ ,  $h_{\text{eff}}^c \equiv h_{\text{eff}}$ , where

$$J_B = \frac{8}{9} \frac{t_2(2t_1 + t_3)}{U} \frac{g_J \mu_B h}{\Delta} j_x^{\uparrow-},$$

$$h_{\text{eff}} = \frac{2}{3} \frac{t_2(t_1 - t_3)}{U} \frac{g_J \mu_B h}{\Delta} j_z^{\uparrow 0} - 24 \frac{(g_J \mu_B h)^3}{\Delta^2} j_x^{\uparrow+} j_z^{\uparrow+} j_x^{\uparrow+}, \quad (3)$$

where  $j_{\alpha}^{\mu\nu} \equiv \langle \mu | J_{\alpha} | \nu \rangle$ ,  $|\uparrow\rangle$  is one of the  $E_g$  states, and  $\{|\pm\rangle, |0\rangle\}$  are the three  $T_{2g}$  states [39]. For the remainder of this Letter we focus on the case of a [111] magnetic field; the general form of  $J_B^{\gamma}$  and  $\mathbf{h}_{\text{eff}}$  for an arbitrary magnetic field direction are given in Sec. II of the SM [39], along with the expressions for  $J_{\tau}$ ,  $J_Q$ , and  $J_O$  previously derived in Ref. [37].

*Classical phase diagrams.* We now explore the phase diagram of the  $J_{\tau} - J_Q - J_O - J_B - h_{\text{eff}}$  model. We study the phase diagram of the Hamiltonian Eq. (2) in the classical limit by treating  $\mathbf{s}$  as an  $O(3)$  vector using Monte Carlo simulated annealing to obtain the classical ground states [40–42]; see Appendix A of Ref. [43] for simulation details. Signatures of quadrupolar and octupolar ordering are given by peaks in the structure factors  $\frac{1}{N} \sum_{ij} (s_i^a s_j^a + s_i^b s_j^b) e^{-i\mathbf{q} \cdot (\mathbf{r}_i - \mathbf{r}_j)}$  and  $\frac{1}{N} \sum_{ij} s_i^c s_j^c e^{-i\mathbf{q} \cdot (\mathbf{r}_i - \mathbf{r}_j)}$ , respectively. We focus on the region where both  $J_{\tau}, J_Q > 0$  by setting  $J_{\tau} = \bar{J} \cos \theta$ ,  $J_Q = \bar{J} \sin \theta \cos \phi$ ,  $J_O = \bar{J} \sin \theta \sin \phi$  and restricting to  $0 \leq \theta \leq \pi/2$ ,  $0 \leq \phi \leq \pi$ ; for  $J_B = 0$  the Hamiltonian is invariant under  $\phi \rightarrow 2\pi - \phi$  (i.e.,  $J_O \rightarrow -J_O$ ) and  $s^c \rightarrow -s^c$  on one of the two honeycomb sublattices. In Fig. 3(a) we present the phase diagram at fixed  $J_B = h_{\text{eff}} = 0$ , which is dominated by the antiferro-octupole (AFO), antiferro-quadrupole (AFQ), ferro-quadrupole (FQ), and vortex-quadrupole (VQ) phases; the VQ phase in particular is a six-site quadrupolar phase; see Sec. III of the SM for pseudospin configuration [39]. Note that each of these phases host either quadrupolar or octupolar

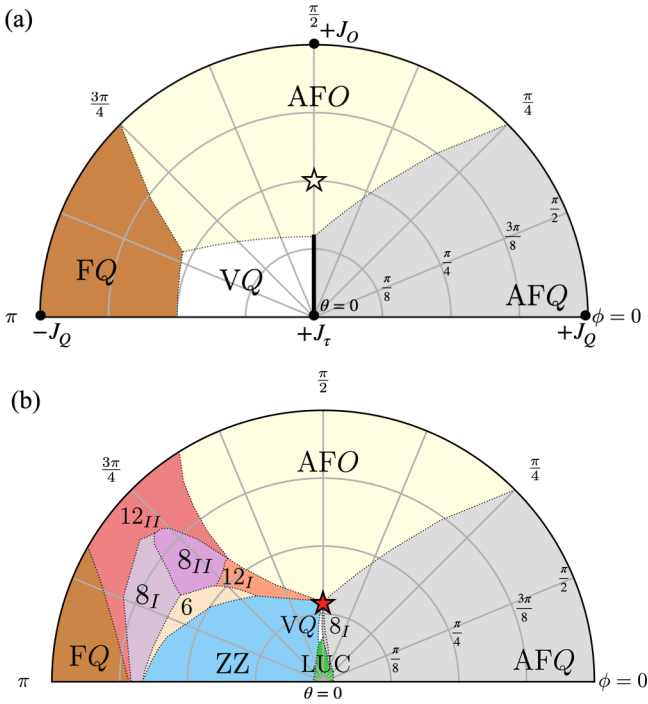


FIG. 3. Classical phase diagrams computed by Monte Carlo simulated annealing at  $h_{\text{eff}} = 0$  and (a)  $J_B = 0$  and (b)  $J_B = \bar{J}/\sqrt{5}$ , where  $\bar{J} = 1$  sets the energy scale. The angles  $(\theta, \phi)$  parametrize the exchange interactions in Eq. (2) as  $J_\tau = \bar{J} \cos \theta$ ,  $J_Q = \bar{J} \sin \theta \cos \phi$ , and  $J_O = \bar{J} \sin \theta \sin \phi$ . Some phases are labeled by the number of sites in the ordering unit cell; two such phases with identical unit cell size are distinguished using Roman numerals. In Sec. III of the SM we display the pseudospin configuration in each ordered phase [39]. The yellow and red stars indicate points shown in Fig. 4; at the red star the Hamiltonian is equivalent to the pure antiferro-Kitaev model.

moments, but not both. The line where  $J_Q = 0$  and  $0 \leq J_O \leq J_\tau/2$  hosts a *disordered* quadrupolar state originating from the pure  $J_\tau$  limit at  $\theta = 0$ . There the model has a macroscopically large ground state manifold owing to the physics of the  $120^\circ$  compass honeycomb model [7,44,45]. The octupolar Ising interaction, which is proportional to  $s_i^\alpha s_j^\alpha$ , does not immediately lift this degeneracy until  $J_O > J_\tau/2$ , where the AFO phase is stabilized in a spin-flop transition. On the other hand, the degeneracy is lifted by finite  $J_Q$  and selects either VQ or AFQ ordering depending on the sign of  $J_Q$ .

In Fig. 3(b) we present the classical phase diagram at a fixed value of  $J_B = \bar{J}/\sqrt{5} > 0$ , which modifies the  $J_B = 0$  case in several notable ways. First, the area surrounding the disordered quadrupolar state in the  $J_B = 0$  limit now hosts several large unit cell (LUC) orders including 24-site and 40-site orders. Second, whereas the region where both  $J_Q, J_O > 0$  is relatively undisturbed, the opposite limit where  $J_Q$  and  $J_O$  differ by a sign hosts a variety of new ordered phases. An example is the zigzag (ZZ) phase which contains both an in-plane and out-of-plane component; see Fig. 4. In fact, all new phases appearing in Fig. 3(b) feature both quadrupolar and octupolar moments; see Sec. III of the SM for a visual representation of the classical pseudospin moments [39]. Third, six different phases emerge from a single point indicated by

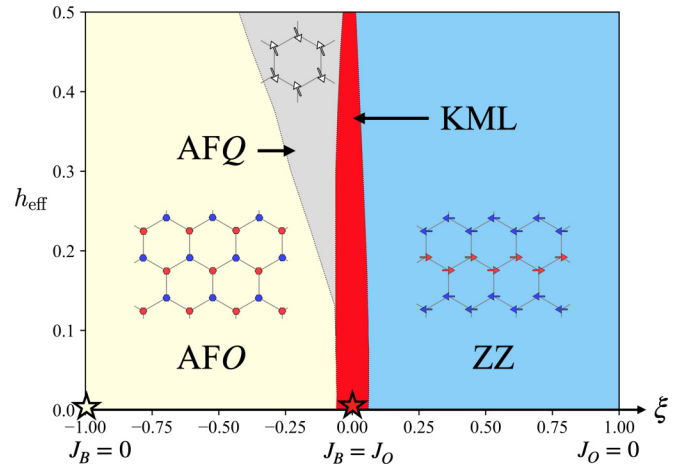


FIG. 4. Quantum phase diagram obtained by 24-site ED, where the parameters  $\xi = (J_B - J_O)/(J_B + J_O)$  and  $h_{\text{eff}}$  are tuned, while  $J_Q = 0$  and  $J_\tau = J_B + J_O = 1$  are fixed. Phase boundaries are given by peaks in the ground state energy derivatives and we determine the presence and type of ordering by calculating the quadrupolar and octupolar structure factors of each phase shown in Sec. III of the SM [39]. The yellow star corresponds to the point where  $J_\tau = J_O$ , whereas the red star corresponds to the antiferro-Kitaev point. For each ordered phase, the arrows represent each pseudospin's in-plane (i.e., quadrupolar) component, whereas red and blue colors indicate the out-of-plane (i.e., octupolar) component with opposite directions.

a red star in Fig. 3(b). In the next section we explore this point in detail and consider the consequences for the quantum pseudospin model.

*Kitaev multipolar liquid.* To find the relation to the Kitaev model, we rewrite the Hamiltonian Eq. (2) in the octahedral  $xy\Gamma$  coordinates, where it may be written in the  $JK\Gamma\Gamma'$  form:

$$H = \sum_{\langle ij \rangle_\gamma} J \mathbf{s}_i \cdot \mathbf{s}_j + K s_i^\gamma s_j^\gamma + \Gamma (s_i^\alpha s_j^\beta + s_i^\beta s_j^\alpha) + \Gamma' [s_i^\gamma s_j^\alpha + s_i^\alpha s_j^\gamma + (\alpha \rightarrow \beta)] - h_{\text{eff}} \sum_i \hat{\mathbf{e}}_c \cdot \mathbf{s}_i, \quad (4)$$

where  $s^\gamma = \hat{\mathbf{e}}_\gamma \cdot \mathbf{s}$ ,  $\gamma \in \{x, y, z\}$ , and  $\alpha, \beta \in \{x, y, z\} \setminus \{\gamma\}$ . The values of  $J$ ,  $K$ ,  $\Gamma$ , and  $\Gamma'$  are given by

$$\begin{aligned} J &= \frac{1}{3} (\frac{1}{2} J_\tau - 2J_B + J_O + 2J_Q), \\ K &= \frac{1}{2} J_\tau + 2J_B, \quad \Gamma = J - J_Q, \\ \Gamma' &= \frac{1}{3} (-J_\tau + J_B + J_O - J_Q). \end{aligned} \quad (5)$$

The special point indicated by the red star in Fig. 3(b) is where  $J_Q = h_{\text{eff}} = 0$  and the other parameters satisfy the ratio  $J_\tau : J_O : J_B = 2 : 1 : 1$ . Here the Hamiltonian takes the form  $H = \sum_{\langle ij \rangle_\gamma} \bar{K} s_i^\gamma s_j^\gamma$ , where  $\bar{K} = 3J_\tau/2 > 0$ ; in other words, our multipolar pseudospin model is described purely by an antiferro-Kitaev interaction. The classical limit of this model hosts an extensive ground state degeneracy, which explains why several classical phases meet at the red star in Fig. 3(b). In analogy to the Kitaev honeycomb model for spin-1/2 moments, we can write the multipolar pseudospin operator in terms of Majorana fermions  $b^\gamma$  and  $c$  as  $s^\gamma = ib^\gamma c/2$ , and the model can be solved exactly in terms of Majorana fermions hopping with a Dirac dispersion in the presence of a

background  $\mathbb{Z}_2$  gauge field. The resulting entangled ground state lacks long-range multipolar order, which we recognize as the KML. The discovery of an exotic phase in an exactly solvable model of multipolar moments in  $d^2$  honeycomb materials forms the central result of this Letter.

We would like to find the ordered multipole phases nearby the KML phase space as  $J_B$  and  $h_{\text{eff}}$  are tuned, as the KML physics may govern the finite temperature above which the multipole ordering melts. To do so, we solve Eq. (2) using ED on the 24-site cluster with the numerical package  $\mathcal{H}\Phi$  [46]. We parametrize the quantum phase diagram by fixing  $J_Q = 0$  and tuning the parameter  $\xi = (J_B - J_O)/(J_B + J_O)$  between  $\xi \in [-1, 1]$ . Whereas  $\xi = -1$  corresponds to the point where  $J_B = 0$  and  $J_\tau = J_O$ , shown in Fig. 3(a) by the yellow star,  $\xi = 0$  corresponds to the point where  $J_B = J_O = J_\tau/2$  which maps to the pure antiferro-Kitaev point. The three ordered phases AFO, AFQ, and ZZ dominate the phase diagram. However, there exists a narrow window where the KML is stabilized which is extended in the  $h_{\text{eff}}$  direction until roughly  $h_{\text{eff}} \sim 0.6J_\tau$ . At the antiferro-Kitaev point, the KML is not immediately susceptible to polarization as the ferro-octupole configuration does not lie within the antiferro-Kitaev ground state manifold.

One may expect that, due to the relations implied by Eq. (5), other ordered phases explored in the  $JK\Gamma\Gamma'$  literature can be stabilized by the model Eq. (2) including the four-site stripy phase. Yet this phase does not appear in our work, as it primarily occupies the  $K < 0$  region [4,6] and we have focused on the region where  $J_\tau, J_B \geq 0$ , i.e.,  $K \geq 0$ . A small stripy phase could appear near  $K > 0$  when  $\Gamma < 0$  and  $\Gamma' > 0$  [25] but it lies outside our parameter space.

*Discussion and summary.* We now discuss the conditions to realize the KML in  $d^2$  insulators. The bond-dependent quadrupole-octupole interaction requires the Zeeman field which induces off-diagonal components between the  $E_g$  and  $T_{2g}$  states while maintaining their energy separation  $\Delta$ ; thus the first condition is that  $g_J\mu_B h \ll \Delta$ . In the  $\text{Os}^{6+}$  and  $\text{Re}^{5+}$  double perovskites  $\Delta$  is around 10–20 meV, restricting  $h \sim \mathcal{O}(10 \text{ T})$ . The second condition is approaching the Kitaev limit. In most edge-sharing materials,  $|t_2|, |t_3| \gg |t_1|$  [6] so that the Kitaev limit is best approached if  $t_2^2 \sim 2t_1t_3$ , since  $J_Q \sim 0$  and  $J_O \sim 4t_2^2/3$  while  $J_\tau \sim 4t_3^2/9$ ; see expressions given in Sec. I of the SM [39]. The ratio of  $t_2$  and  $t_3$  then

determines whether the material is VQ, AFQ, or AFO ordered in the zero-field limit shown in Fig. 3(a). As the magnetic field is introduced and  $J_B$  is increased, the system approaches the KML phase space but it may remain in the ordered phase depending on  $t_2/t_3$ . The signature of KML physics is then revealed at the finite temperatures above which the ordering vanishes. The intricate balance between the field strength  $h/\Delta$  and exchange paths presents a challenge for the material realization of the KML. Nevertheless, this work serves as a “proof of concept” that the  $d^2$  spin-orbit entangled honeycomb insulators with non-Kramers doublets may exhibit multipolar Kitaev physics.

In this Letter we have shown that the KML can arise in a spin-orbit coupled  $d^2$  honeycomb material. The key ingredient is the application of a magnetic field which allows for bond-dependent quadrupole-octupole interactions in the effective Hamiltonian of the  $E_g$  doublet. In combination with the Ising octupole and  $120^\circ$  compasslike quadrupole terms, the Hamiltonian can be tuned to the pure Kitaev form. The resulting multipolar model can then be solved exactly using Majorana fermions, in analogy with Kitaev’s original spin-1/2 model. Multipolar ordered phases arise along with the KML, including those featuring combinations of quadrupolar and octupolar ordering, as well as a disordered compass-quadrupole phase. The nature and extent of these phases in the quantum phase diagram form interesting avenues of future work. We have also shown that the field-induced bond-dependent  $J_B$  becomes bond anisotropic when the field is tilted away from the  $c$  axis. This extended phase space, and the novel physics contained within, motivates future studies of  $d^2$  multipolar systems.

*Acknowledgments.* A.R. thanks P. P. Stavropoulos, S. Voleti, and F. D. Wandler for helpful discussions. We acknowledge support from the Natural Sciences and Engineering Research Council of Canada Discovery Grant No. 2022-04601. H.Y.K. also acknowledges support from the Canadian Institute for Advanced Research and the Canada Research Chairs Program. Computations were performed on the Niagara supercomputer at the SciNet HPC Consortium. SciNet is funded by the Canada Foundation for Innovation under the auspices of Compute Canada, the Government of Ontario, Ontario Research Fund–Research Excellence, and the University of Toronto.

- 
- [1] A. Y. Kitaev, *Ann. Phys. (NY)* **303**, 2 (2003).  
 [2] A. Kitaev, *Ann. Phys. (NY)* **321**, 2 (2006).  
 [3] G. Jackeli and G. Khaliullin, *Phys. Rev. Lett.* **102**, 017205 (2009).  
 [4] J. Chaloupka, G. Jackeli, and G. Khaliullin, *Phys. Rev. Lett.* **105**, 027204 (2010).  
 [5] W. Witczak-Krempa, G. Chen, Y. B. Kim, and L. Balents, *Annu. Rev. Condens. Matter Phys.* **5**, 57 (2014).  
 [6] J. G. Rau, E. K.-H. Lee, and H.-Y. Kee, *Phys. Rev. Lett.* **112**, 077204 (2014).  
 [7] Z. Nussinov and J. van den Brink, *Rev. Mod. Phys.* **87**, 1 (2015).  
 [8] J. G. Rau, E. K.-H. Lee, and H.-Y. Kee, *Annu. Rev. Condens. Matter Phys.* **7**, 195 (2016).  
 [9] S. M. Winter, A. A. Tsirlin, M. Daghofer, J. van den Brink, Y. Singh, P. Gegenwart, and R. Valentí, *J. Phys.: Condens. Matter* **29**, 493002 (2017).  
 [10] Y. Motome, R. Sano, S. Jang, Y. Sugita, and Y. Kato, *J. Phys.: Condens. Matter* **32**, 404001 (2020).  
 [11] T. Takayama, J. Chaloupka, A. Smerald, G. Khaliullin, and H. Takagi, *J. Phys. Soc. Jpn.* **90**, 062001 (2021).  
 [12] S. Trebst and C. Hickey, *Phys. Rep.* **950**, 1 (2022).  
 [13] K. W. Plumb, J. P. Clancy, L. J. Sandilands, V. V. Shankar, Y. F. Hu, K. S. Burch, H.-Y. Kee, and Y.-J. Kim, *Phys. Rev. B* **90**, 041112(R) (2014).  
 [14] H.-S. Kim, Vijay Shankar V., A. Catuneanu, and H.-Y. Kee, *Phys. Rev. B* **91**, 241110(R) (2015).

- [15] A. Koitzsch, C. Habenicht, E. Müller, M. Knupfer, B. Büchner, H. C. Kandpal, J. van den Brink, D. Nowak, A. Isaeva, and T. Doert, *Phys. Rev. Lett.* **117**, 126403 (2016).
- [16] L. J. Sandilands, Y. Tian, A. A. Reijnders, H.-S. Kim, K. W. Plumb, Y.-J. Kim, H.-Y. Kee, and K. S. Burch, *Phys. Rev. B* **93**, 075144 (2016).
- [17] X. Zhou, H. Li, J. A. Waugh, S. Parham, H.-S. Kim, J. A. Sears, A. Gomes, H.-Y. Kee, Y.-J. Kim, and D. S. Dessau, *Phys. Rev. B* **94**, 161106(R) (2016).
- [18] A. Banerjee, C. A. Bridges, J.-Q. Yan, A. A. Aczel, L. Li, M. B. Stone, G. E. Granroth, M. D. Lumsden, Y. Yiu, J. Knolle, S. Bhattacharjee, D. L. Kovrizhin, R. Moessner, D. A. Tennant, D. G. Mandrus, and S. E. Nagler, *Nat. Mater.* **15**, 733 (2016).
- [19] H.-S. Kim and H.-Y. Kee, *Phys. Rev. B* **93**, 155143 (2016).
- [20] S. M. Winter, Y. Li, H. O. Jeschke, and R. Valentí, *Phys. Rev. B* **93**, 214431 (2016).
- [21] L. Janssen, E. C. Andrade, and M. Vojta, *Phys. Rev. B* **96**, 064430 (2017).
- [22] W. Wang, Z.-Y. Dong, S.-L. Yu, and J.-X. Li, *Phys. Rev. B* **96**, 115103 (2017).
- [23] P. Laurell and S. Okamoto, *npj Quantum Mater.* **5**, 2 (2020).
- [24] Y. Singh, S. Manni, J. Reuther, T. Berlijn, R. Thomale, W. Ku, S. Trebst, and P. Gegenwart, *Phys. Rev. Lett.* **108**, 127203 (2012).
- [25] J. G. Rau and H.-Y. Kee, [arXiv:1408.4811](https://arxiv.org/abs/1408.4811).
- [26] S. Hwan Chun, J.-W. Kim, J. Kim, H. Zheng, C. Stoumpos, C. Malliakas, J. Mitchell, K. Mehlawat, Y. Singh, Y. Choi, T. Gog, A. Al-Zein, M. Sala, M. Krisch, J. Chaloupka, G. Jackeli, G. Khaliullin, and B. J. Kim, *Nat. Phys.* **11**, 462 (2015).
- [27] S. C. Williams, R. D. Johnson, F. Freund, S. Choi, A. Jesche, I. Kimchi, S. Manni, A. Bombardi, P. Manuel, P. Gegenwart, and R. Coldea, *Phys. Rev. B* **93**, 195158 (2016).
- [28] H. Liu and G. Khaliullin, *Phys. Rev. B* **97**, 014407 (2018).
- [29] R. Sano, Y. Kato, and Y. Motome, *Phys. Rev. B* **97**, 014408 (2018).
- [30] H. Liu, J. Chaloupka, and G. Khaliullin, *Phys. Rev. Lett.* **125**, 047201 (2020).
- [31] M. Songvilay, J. Robert, S. Petit, J. A. Rodriguez-Rivera, W. D. Ratcliff, F. Damay, V. Balédent, M. Jiménez-Ruiz, P. Lejay, E. Pachoud, A. Hadj-Azzem, V. Simonet, and C. Stock, *Phys. Rev. B* **102**, 224429 (2020).
- [32] A. Paramekanti, D. D. Maharaj, and B. D. Gaulin, *Phys. Rev. B* **101**, 054439 (2020).
- [33] D. D. Maharaj, G. Sala, M. B. Stone, E. Kermarrec, C. Ritter, F. Fauth, C. A. Marjerrison, J. E. Greedan, A. Paramekanti, and B. D. Gaulin, *Phys. Rev. Lett.* **124**, 087206 (2020).
- [34] S. Voleti, D. D. Maharaj, B. D. Gaulin, G. Luke, and A. Paramekanti, *Phys. Rev. B* **101**, 155118 (2020).
- [35] G. Khaliullin, D. Churchill, P. P. Stavropoulos, and H.-Y. Kee, *Phys. Rev. Res.* **3**, 033163 (2021).
- [36] S. Voleti, A. Haldar, and A. Paramekanti, *Phys. Rev. B* **104**, 174431 (2021).
- [37] D. Churchill and H.-Y. Kee, *Phys. Rev. B* **105**, 014438 (2022).
- [38] G. Chen and L. Balents, *Phys. Rev. B* **84**, 094420 (2011).
- [39] See Supplemental Material at <http://link.aps.org/supplemental/10.1103/PhysRevB.107.L020408> for the derivation of the effective pseudospin Hamiltonian for arbitrary magnetic field directions, the definition of the  $E_g/T_{2g}$  states, and the representation of the Zeeman field in this basis. It also includes pseudospin configurations obtained by classical Monte Carlo as well as structure factors obtained by 24-site exact diagonalization.
- [40] N. Metropolis, A. W. Rosenbluth, M. N. Rosenbluth, A. H. Teller, and E. Teller, *J. Chem. Phys.* **21**, 1087 (1953).
- [41] S. Kirkpatrick, Jr., C. D. Gelatt, and M. P. Vecchi, *Science* **220**, 671 (1983).
- [42] S. Kirkpatrick, *J. Stat. Phys.* **34**, 975 (1984).
- [43] A. Rayyan, Q. Luo, and H.-Y. Kee, *Phys. Rev. B* **104**, 094431 (2021).
- [44] C. Wu, *Phys. Rev. Lett.* **100**, 200406 (2008).
- [45] J. Nasu, A. Nagano, M. Naka, and S. Ishihara, *Phys. Rev. B* **78**, 024416 (2008).
- [46] M. Kawamura, K. Yoshimi, T. Misawa, Y. Yamaji, S. Todo, and N. Kawashima, *Comput. Phys. Commun.* **217**, 180 (2017).